COMMUNICATION

Check for updates

Chemical exfoliation of 1-dimensional antiferromagnetic nanoribbons from a non-van der Waals material†

Mulan Yang, [a] Guangming Cheng, [b] Nitish Mathur, [a] Ratnadwip Singha, [a] Fang Yuan, [a] Nan Yao [b] and Leslie M. Schoop *[a]

As the demand for increasingly varied types of 1-dimensional (1D) materials grows, there is a greater need for new methods to synthesize these types of materials in a simple and scalable way. Chemical exfoliation is commonly used to make 2-dimensional (2D) materials, often in a way that is both straightforward and suitable for making larger quantities, yet this method has thus far been underutilized for synthesizing 1D materials. In the few instances when chemical exfoliation has been used to make 1D materials, the starting compound has been a van der Waals material, thus excluding any structures without these weak bonds inherently present. We demonstrate here that ionically bonded crystals can also be chemically exfoliated to 1D structures by choosing $KFeS_2$ as an example. Using chemical exfoliation, antiferromagnetic 1D nanoribbons can be yielded in a single step. The nanoribbons are crystalline and closely resemble the parent compound both in structure and in intrinsic antiferromagnetism. The facile chemical exfoliation of an ionically bonded crystal shown in this work opens up opportunities for the synthesis of both magnetic and non-magnetic 1D nanomaterials from a greater variety of starting structures.

New concepts

Chemical exfoliation is a scalable and facile synthesis technique for making nanomaterials, as evidenced by the many 2-dimensional materials that have been made in this way. However, despite the utility of this method, chemical exfoliation has rarely been applied to the synthesis of 1-dimensional (1D) materials. A few studies have shown that nanowires can be exfoliated from quasi-1D van der Waals materials, but we seek to broaden the applicability of chemical exfoliation to many other 1D materials by removing this limitation. Using $KFeS_2$ as a case study, we show that quasi-1D crystal structures containing ionically bonded chains can be exfoliated to make nanoribbons of the same structure. Using transmission electron microscopy, we also determined the mechanism by which the nanoribbons form. The resultant nanomaterials also maintain the intrinsic antiferromagnetism of the parent compound, confirming that liquid exfoliation does not eliminate magnetism from the system. We hope this example emboldens researchers to use chemical exfoliation when trying to synthesize all manner of 1D materials; a van der Waals bonded structure is no longer a prerequisite.

Introduction

The development of new nanomaterials has given rise to a variety of possible applications and theoretical studies, generally due to their high surface area-to-volume ratio and possible changes in their properties due to quantum confinement effects.[1,2] These materials are categorized by their dimensionality, *i.e.*, 2-dimensional (2D) materials are nanoscale in one dimension, 1-dimensional (1D) materials in two, and 0-dimensional (0D) materials in all three.[3] Materials such as nanowires and

nanoribbons are categorized as 1D and can be used in sensing,[4] catalysis,[5] and filtration.[6] Magnetic nanowires have further uses as nanobarcodes,[7] detectors of biopolymers,[8] spintronic devices,[9,10] data storage,[11] and as model materials for unconventional physics, such as magnetic frustration[12] and curvature-induced changes in magnetic field textures.[13]

Given this widespread interest, scalable methods that are applicable to a broad range of 1D structures are needed. Currently, one of the most common syntheses involves using metal nanoparticles, either in the liquid or solid phase, to catalyze the bottom-up growth of nanowires.[14,15] Potential issues arise if a metal nanoparticle used as a catalyst is incorporated into the nanowire.[16] Doping the materials as they are grown can also be difficult due to issues such as the different rates of incorporation of different elements.[14] There are top-down approaches, including lithography, that can circumvent these challenges by first growing the material as a bulk crystal. However, this limits the materials to thermodynamically stable phases that often need to be lattice matched with the substrate

[a] *Department of Chemistry, Princeton University, Princeton, NJ 08544, USA.*
E-mail: lschoop@princeton.edu

[b] *Princeton Materials Institute, Princeton, NJ 08544, USA*

to avoid defects or dislocations from strain.[14] An alternate synthetic route is chemical exfoliation, which has the advantage of being tunable to a wide range of materials, high yielding, and structurally consistent in its products.[1] In addition, this solution processing method can be used to make inks of nanomaterials with magnetic and electronic properties of interest for applications like thin-film transistors and flexible electronics.[17–19]

Even though chemical exfoliation methods have been developed for synthesizing a wide variety of 2D materials, these methods have yet to be commonly applied to 1D materials.[20] In the rare instances where liquid exfoliation is used, the starting materials are vdW compounds and have clear cleavage planes at these weak bonds. The first use of liquid exfoliation to make nanowires (as opposed to the simple dispersal of bulk material into solution)[21] was in 2018 when Tian *et al.* made KP_{15} nanowires by sonication in ethanol. Although the bulk structure of KP_{15} incorporates both vdW and ionic bonding between the chains, the authors indicated that the cleavage into nanowires occurred at the vdW gaps between the planes.[22] The next usage of chemical exfoliation was by Liu *et al.* in 2020, who used a similar sonication method to make semiconducting nanowires from the vdW material $Ta_2Pd_3Se_8$.[23] Qu *et al.* extended this method in 2021 to the magnetic vdW material $CrSbSe_3$.[20] They were able to synthesize high-quality nanowires that notably also retained the magnetic properties of the bulk material.

The library of accessible 1D materials would expand greatly if we could chemically exfoliate 1D nanostructures from materials with bonds stronger than those in vdW compounds. Non-vdW compounds, including Bi_2O_2Se,[24] $Na_3Ni_2BiO_6$,[25] $NaCrS_2$,[26] and FeF_3,[27] have previously been chemically exfoliated to 2D sheets and platelets. By utilizing a wet ball-milling technique, even the covalently-bonded crystal α-germanium could be delaminiated into nanolayers.[28] Certain materials, such as α-Fe_2O_3[29] and $FeTiO_3$,[30] retain their magnetic ordering even after undergoing liquid exfoliation. In addition, the non-vdW crystal $RbNbO_3$ has been chemically exfoliated to make $H_xRb_{1-x}O_3$ "nanobelts," which suggests that extending this technique to 1D is possible.[31] Another study showed that $Li_2Mo_6Se_6$, which is a quasi-1D compound, can be dispersed in anhydrous methanol to produce nanowires of MoSe, although the process is hampered by the air and moisture sensitivity of the crystals.[32] Given this precedent, we investigated the possibility of applying similar techniques under ambient conditions to an ionically bonded, quasi-1D chain compound and chose to study $KFeS_2$, which has chains made of edge-sharing FeS_4 tetrahedra that are ionically bonded by K^+ (Fig. 1). Previous work has shown that $KFeS_2$ nanowires can be synthesized using a bottom-up method, which requires the nanowires to be anchored to an Fe foam.[33] An alternative bottom-up synthesis in solution results in "whiskers" of $KFeS_2$.[34]

In addition to determining the feasibility of using liquid exfoliation to make these compounds, we also sought to determine whether the magnetic properties could be preserved. Magnetic studies on bulk $KFeS_2$ show that it is antiferromagnetic (AFM) within the chains, with a Néel temperature (T_N) of 250 ± 5 K; there are ferromagnetic (FM) interactions between

Fig. 1 Structure of $KFeS_2$. Notice the quasi-1D chain motif, with ionic bonds to an alkali ion.

the chains, but due to the significantly larger spacing between inter-chain Fe ions (6.6 Å) *versus* intra-chain Fe ions (2.7 Å), these interactions are less significant.[35–39] Because the main magnetic interactions take place within the chain, the exfoliation process should not disrupt them greatly.

In this work, we implement a simple chemical exfoliation method to synthesize free-standing, crystalline $KFeS_2$ nanoribbons and nanosheets. Note that we use "nanoribbon" here instead of "nanowire" to describe these 1D materials to clarify that their cross-section is flatter compared to most nanowires, following the terminology of Kong *et al.*[40] However, unlike the nanowires and nanoribbons they grew, the crystal growth direction of these nanoribbons is the same as that of the previously referenced $KFeS_2$ nanowires.[33] The nanoribbons may be more easily related to the structures commonly formed from transition metal dichalcogenides as well.[41] We show the variety of morphologies that can be formed and offer mechanistic reasoning for this behavior elucidated from electron diffraction imaging of individual samples. We also show that post-exfoliation, these materials retain their AFM character, albeit with a decrease in the Néel temperature. A magnetic hysteresis occurs in the nanostructures that is not present in the bulk material, potentially due to sulfur vacancies or other factors that cause uncompensated magnetic moments.[42,43]

Results and discussion

To investigate the mechanism by which ionically bonded crystals can be chemically exfoliated to 1D nanomaterials, we chose to study $KFeS_2$ as a model. This material was chosen for its structure, as seen in Fig. 1, which is suitable for exfoliation to 1D as it consists of FeS_4 chains that run along the *c*-axis with K^+ ions in between to hold the chains together. This is reminiscent of materials in the A_xMS_2 family, where A = Li, Na, K and M = Mo, W, Nb, Ta, Ti, that have been chemically exfoliated to ultrathin 2D nanosheets.[44,45] These A ions tend to react readily with water, which can facilitate exfoliation through the intercalation of water molecules to separate the layers.[31,46] In MAX phases, which are similarly layered and non-vdW, the M–A bond is

Fig. 2 When (a) bulk $KFeS_2$ is sonicated in $1:2$ IPA/H_2O for 90 min, it exfoliates into a mixture of (b) nanosheets and (c) nanoribbons, as well as occasional (d) particularly long nanoribbons. Although the morphologies are different, they all share the same crystal structure, as confirmed by the (b)–(d) insets) selected area electron diffraction patterns indexed to the [010] zone axis. The (002) diffraction spot is circled in cyan and the (200) is circled in yellow. The scale bar represents 5 nm^{-1}. Note that the patterns have been rotated to the same direction for ease of comparison.

known to be more reactive than the M–S bond, which allows the M–A bond to be broken preferentially during exfoliation.[46,47] Assuming these bonds behave similarly in their 1D counterparts, we propose that during exfoliation the crystals will cleave K–S bonds before Fe–S bonds, leaving the chains intact. Therefore, the two possible cleavage planes are between the chains, along the *ac* or *bc* planes, which are equivalent to the (010) and (100) planes respectively. Because the K–S bonds required to break are nearly identical in length (3.34 Å and 3.31 Å, respectively), the crystals should cleave at both planes with perhaps a slight preference for cleaving at the *ac* plane.

Nanomaterials were successfully synthesized by sonicating bulk $KFeS_2$ (Fig. 2a) in a $1:2$ solution of isopropyl alcohol (IPA) and water for 90 min. Two rounds of centrifugation were performed to isolate the exfoliated materials from any remaining bulk material and the resultant solids were dried under vacuum (details under Materials and Methods). Approximately 0.5–1 mg of nanomaterials was synthesized from each exfoliation of approximately 35 mg of bulk $KFeS_2$. Both bulk and

exfoliated $KFeS_2$ are slightly water sensitive and so the materials were stored under argon when not in use to prevent oxidation. Post-exfoliation, we consistently observed both nanoribbon and nanosheet morphologies. To determine their crystal structures and properties, we used several characterization methods including diffraction, microscopy, and magnetic measurements. The samples were sufficiently air-stable for characterization to be done under atmospheric conditions. To establish the applicability of similar exfoliation methods to other quasi-1D chain compounds, we performed preliminary experiments on bulk $KSbS_2$ (Fig. S1, ESI†) and showed that nanostructures could be exfoliated from this material as well (Fig. S2, ESI†), although further optimization to obtain smaller particles is necessary in this case. The exfoliation method and possible cleavage mechanism are described in the ESI.†

The rest of this work focuses solely on the results from exfoliating $KFeS_2$. An ensemble of nanomaterials was collected by centrifuging the exfoliation mixture and removing the supernatant. Powder X-ray diffraction (PXRD) data (Fig. 3) on such an ensemble confirmed that the exfoliation process did not affect the structure. Rietveld refinement of the PXRD shows that it matches well with the parent structure (R_{wp} = 5.9%). Although there is no clear change in peak shape, which can be an indication of the nanoscale nature of a material, high-angle annular dark-field scanning transmission electron microscope (HAADF-STEM) images of the PXRD sample (Fig. S3a, ESI†) showed successful exfoliation.

Transmission electron microscopy (TEM) and HAADF-STEM were also used to visualize the different morphologies of the $KFeS_2$ nanomaterials. A statistical analysis was performed on 237 individual samples to determine the distribution of nanostructures (Fig. S4, ESI†). These categories were defined by their aspect ratios: greater than 5 (1D nanoribbons) and less than 5 (2D nanosheets) (Fig. 2b and c). The aspect ratios ranged from approximately 1 to 88, so the nanoribbon group includes extra "long" nanoribbons (Fig. 2d). Over half (59%) of the exfoliated materials were nanoribbons and the rest were nanosheets. Energy-dispersive X-ray spectroscopy (EDX) shows a near $1:1:2$ stoichiometry of K:Fe:S regardless of the morphology (Fig. S5, ESI†) and no impurities were found.
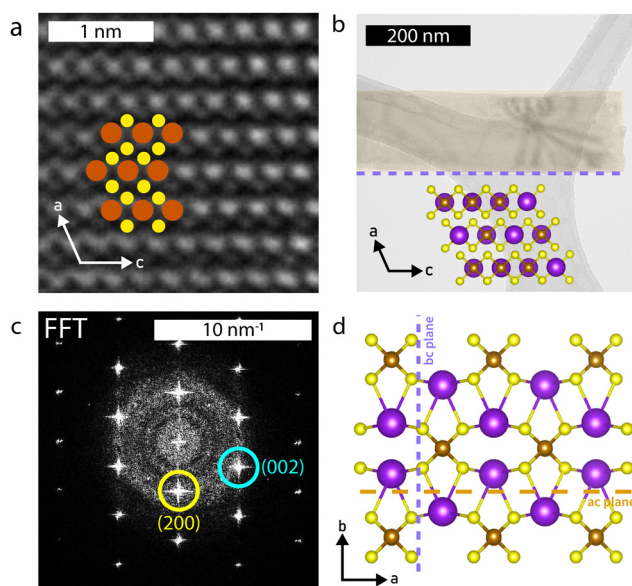

Fig. 3 PXRD data of the exfoliated $KFeS_2$ agrees well with the Rietveld refinement data.
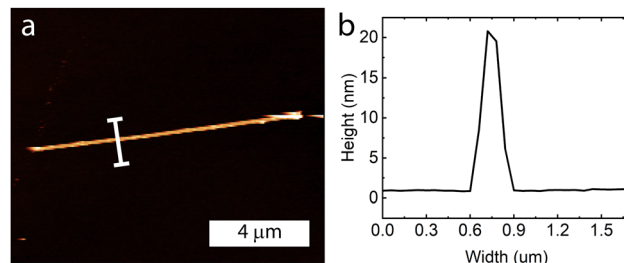
Selected area electron diffraction (SAED) images (Fig. (2b–d) insets) confirm the structure to be that of the parent compound; the measured d-spacings are within 3% of the known structure (Table S3, ESI†) and the pattern matches SAED images from $KFeS_2$ nanowires grown by Li et al.[33] SAEDs were taken on samples of each morphology to confirm that they all share the same structure. High resolution (HR)-TEM further corroborates this result, as shown in Fig. 4a. The pattern of atoms matches that of $KFeS_2$ as seen from the b-axis (Fig. 4b inset) and the fast Fourier transform (FFT) (Fig. 4c) indexes to the same peaks as the SAED. The measured atomic spacings are also within 3% error of the known values.

The SAED patterns additionally give insight into the mechanism of formation of different morphologies of $KFeS_2$ (Fig. 4d). Most of the patterns show the ac plane of the material. This suggests that one of the easiest cleavage planes is the ac plane, which agrees with the prediction based on bond distances as discussed previously. By cleaving here, nanosheets of the material are generated. However, as mentioned above, it should be similarly easy to cleave along the bc plane. As suspected, cleavage occurs at the bc plane in addition to the ac plane, resulting in nanoribbons. In a few SAEDs (Fig. S3c, ESI†), the bc plane is visible, which supports this being the other cleavage plane. By measuring the distance between diffraction spots, we see that the Fe–Fe distance within the chain is within 3% of that of the parent structure. However, the inter-chain Fe–Fe distance has decreased significantly (Table S4, ESI†), which may be due to a loss of K^+ ($\sim$6%–20%) during the exfoliation process that causes the chains to collapse towards each other.

Fig. 5 (a) Atomic force microscopy image of a nanoribbon, with (b) the height profile showing it is approximately 20 nm in height.

Although this structural change is not seen in the XRD data, the SAED confirms its occurrence in this particular sample, as the SAED pattern shown in Fig. S3c (ESI†) was taken directly from the sample used for XRD. The effect may be too minimal to be seen on XRD, but detectable by more sensitive techniques, as seen in the magnetic data.

Atomic force microscopy was performed on individual nanoribbons to determine the average thickness of these samples (Fig. 5 and Fig. S6, ESI†). The samples ranged from 20–30 nm in height and were fairly uniform along the entire sample length.

To investigate if the magnetic properties of $KFeS_2$ were retained post-exfoliation, magnetic susceptibility measurements were performed at 500 Oe on bulk (Fig. 6a) and an ensemble of exfoliated $KFeS_2$ (Fig. 6b). The bulk data is comparable to literature results from powder samples; there is no obvious transition at T_N, but there is a broad, higher temperature ($T = 353$ K) transition that was also previously observed and had been

Fig. 4 (a) HR-TEM image showing arrangement of atoms within the nanoribbon. (b) TEM image of a nanoribbon, showing cleavage along both ac and bc planes, as well as the atomic structure viewed along the b-axis. (c) The FFT of (a) indexed along the [010] zone axis. (d) Cleavage planes in $KFeS_2$. Cleavage along the ac plane (orange, dashed line) exfoliates the bulk crystal to a 2D structure and cleavage along the bc plane (purple, dotted line) further reduces the crystal to a 1D structure.
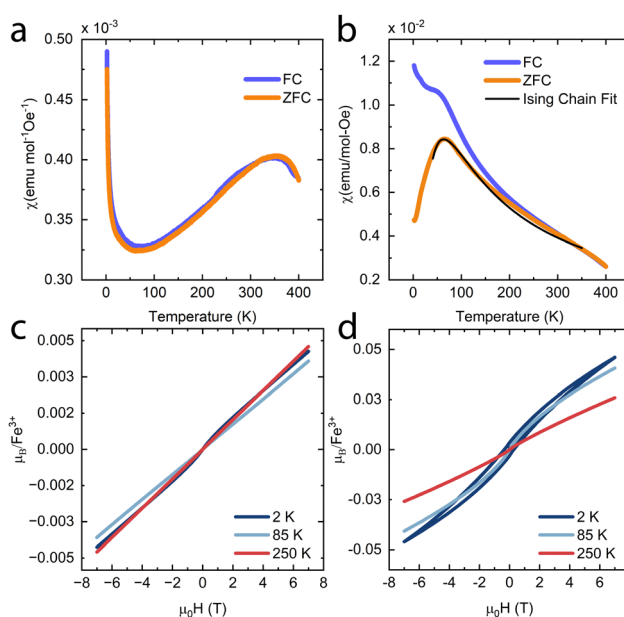

Fig. 6 Magnetic susceptibility data at 500 Oe of (a) bulk and (b) exfoliated $KFeS_2$. The exfoliated $KFeS_2$ zero-field-cooled data (ZFC) has been fit as an Ising chain, shown in black. Field-dependent magnetization data of (c) bulk and (d) exfoliated $KFeS_2$ is also shown; note the hysteresis at $T = 2$ K that occurs only in the exfoliated sample. Additional data shown was collected at possible temperatures of interest: $T = 85$ K (broad peak) and $T_N = 250$ K.

attributed to short range correlations occurring above T_N.[37,38] Literature measurements agree that this broad peak is present, but show it occurring at a range of temperatures: 565 K in a single crystal sample[38] and closer to 700 K in a powder sample.[35] The susceptibility of the ensemble of exfoliated nanostructures shows a similar broad peak, which could be attributed to either of two causes. This peak may be due to the same short range interactions causing the broad peak seen in the bulk data, but the AFM transition in quasi-1D compounds is also known to be broader than ones seen in 3D compounds.[48–50] In either case, the dramatic decrease in the temperature at which this peak occurs indicates that there is a decrease in the T_N. Sulfur vacancies may be limiting the amount of AFM interactions between the Fe ions by disrupting the superexchange mechanism, thus reducing the AFM character.[42] Any decrease in distance between the chains could also encourage more inter-chain FM interactions to occur, which may disrupt the intra-chain AFM interactions as well. The bifurcation of the field-cooled (FC) data may be due to superparamagnetism of sparse iron impurities.[51,52]

The magnetic susceptibility data of quasi-1D AFM chain compounds is usually fit using either the Heisenberg model (in the form of the Bonner–Fisher equation)[48] or the Ising model. We also tried to fit the data to the Curie–Weiss law (Fig. S7, ESI†), but the high-temperature data is non-linear; one cause of this may be a small peak at $T = 350$ K from residual bulk material. The best fit for the zero-field-cooled (ZFC) data of the exfoliated materials was to eqn (1) for a spin-5/2 Ising model. This equation was adapted from Keene et al., who found it to model the behavior of Fe(II) more accurately than does the Bonner–Fisher equation because it better accounted for iron-specific qualities such as strong spin–orbit coupling.[53] This choice is also supported by Sweeney and Coffman, who showed that KFeS$_2$ appeared to fit better to an Ising model than to the Heisenberg model.[54]

$$\chi = \frac{N_A g^2 \mu_B^2 S(S+1)}{3k_B T} \cdot \exp\left(\frac{4J}{k_B T}\right) \qquad (1)$$

In eqn (1), N_A is Avogadro's number, S is the spin state, μ_B is the Bohr magneton, and k_B is the Boltzmann constant. We solve for g, the g-factor of the magnetic ion, and J, the intra-chain exchange constant. It was determined that $J/k_B = -16$ K and $g = 1.2$ in the nanoribbon/nanosheet ensemble. The published g-factor of bulk KFeS$_2$ is 2.0,[55] so this value is significantly lower than expected. There are multiple possibilities for why this value differs so greatly from the previously measured value: Fe being difficult to fit, as Keene et al. had stated,[53] and possible variation in the Fe oxidation state due to slight loss of K or S during the exfoliation process, which would differ from the model which assumes a spin-5/2 state. Although this calculated g-factor is low, we will continue with this model as it gave the best fit and discuss the resultant values in a general sense.

Previous studies of single crystal KFeS$_2$ have used a spin-1/2 Heisenberg model to calculate J/k_B to be -441 K,[36,38] but a spin-5/2 Heisenberg model on a powder sample resulted in a very different J/k_B of -66 K.[35] Overall, the absolute value is always

higher for the bulk than what is reported here for the nanostructures, indicating a greater intra-chain Fe–Fe exchange interaction in the bulk than in the exfoliated material. This agrees with the lower AFM character of the nanomaterials. Using the Green function method from Oguchi,[56] we estimate that the ratio of inter- to intra-chain exchange is slightly less than 1. This value is higher than that reported for the bulk, which is on the order of 0.1,[35,36] perhaps due to the increase in inter-chain interactions from the chains getting closer together.

Field-dependent magnetization measurements on bulk KFeS$_2$ (Fig. 6c) show AFM ordering with a minor FM impurity, most likely some form of Fe such as KFeO$_2$.[39] When measuring the nanostructure ensemble (Fig. 6d), however, a small hysteresis opens up, which has multiple possible causes. Because the chains interact FM with each other, it is possible that the weakened AFM interactions allow the FM interactions between the chains to become more prominent. Although not seen in the overall PXRD of the exfoliated samples, the chains may also be closer to each other in some nanostructures, as seen in the occasional SAED of a nanoribbon, which would also increase the FM interactions. Alternatively, the hysteresis may be caused by uncompensated magnetic moments which taken together appear FM. These may result from sulfur vacancies weakening the AFM interactions.[42] Finally, another possible explanation is the development of spin-glass-like behavior. In the closely related material KFeO$_2$, competition between the major AFM state and a small FM component can lead to spin-glass behavior presenting as hysteresis in the magnetization measurements. This behavior may be the result of geometric frustration or uncompensated spins on the surface of the material.[43] The development from an AFM state to a spin-glass-like one may be exacerbated by the exfoliation to nanoscale dimensions, as this transition has been observed in nanostructures such as LaFeO$_3$ nanoparticles[57] and hollow γ-Fe$_2$O$_3$ nanoparticles.[58] Overall, however, the AFM behavior is retained. The small measured magnetic moments also support this. The higher moment of the nanostructures may be attributed to a greater Fe impurity, but the magnetic moment is still significantly lower than what would be expected in a FM material. In general, the analysis of the magnetic properties shows that, although differing from the bulk, magnetic order is retained in the exfoliated nanostructures.

Conclusions

We have shown here that in the synthesis of 1D nanostructures, liquid exfoliation is not limited solely to layered vdW materials, but can instead be extended to synthesize 1D materials from a variety of chain-containing crystals, including those that are magnetic and ionically bonded. The quasi-1D compound KFeS$_2$ was exfoliated into nanoribbons averaging 25 nm in height. The exfoliation was facile and resulted in a majority of nanoribbons, thus making them simple to mass-produce. Magnetic measurements showed that the exfoliated materials retain AFM behavior with the T_N lower compared to that of the bulk. A small magnetic hysteresis opens up in the exfoliated material, which

may be due to sulfur vacancies slightly disrupting the AFM state and causing some magnetic moments to become uncompensated. Having shown the efficacy of this technique for making $KFeS_2$ nanoribbons, as well as preliminary work on making $KSbS_2$ nanostructures, we encourage other researchers to employ this method in the synthesis and study of 1D nanostructures from any chain-containing, quasi-1D compounds.

Materials and methods

Synthesizing $KFeS_2$

Bulk $KFeS_2$ was synthesized using a $1:0.8:2$ molar ratio of potassium (cubes in mineral oil, Oakwood Chemical), iron ($\geq$ 99%, reduced, powder (fine), Sigma Aldrich), and sulfur (powder, sublimed, -100 mesh, 99.5%, Alfa Aesar). The reagents were loaded into an alumina crucible under an argon atmosphere and sealed inside a quartz tube under vacuum. This was heated to 700 °C at 90 °C h^{-1} and held at this temperature for 5 days. It was then cooled at 25 °C h^{-1} to 300 °C before cooling to room temperature.

Exfoliating $KFeS_2$

Nanoribbons and nanosheets were exfoliated from bulk $KFeS_2$ in a $1:2$ IPA:H_2O solution, similar to the method used by Qu et al.[20] The powder was added at 1.2 mg mL^{-1} and the mixture was then sonicated for 90 min on low power using a sonicator (Branson CPX1800). To minimize possible oxidation of $KFeS_2$ in water, the mixture was then centrifuged (Sigma 3-30KS) at 14 000 rpm for 45 min to collect all of the material at the bottom of the tube. Most of the solvent was removed and was replaced with 21 mL of IPA. The nanostructures were redispersed by sonicating for 5 min. To remove any remaining bulk $KFeS_2$, the mixture was centrifuged at 2000 rpm for 10 min and the supernatant from this step was centrifuged at 3000 rpm for a further 10 min. Finally, to collect the exfoliated materials, the liquid was centrifuged at 13 000 rpm for 30 min. The nanostructures were dried under vacuum to ensure no solvent remained.

Characterization

Structures were visualized using the software VESTA.[59] For PXRD, the dried nanomaterials were collected into a 0.5 mm capillary. The powder diffractometer (STOE STADI P) used Mo Kα 1 radiation and a Dectris Mythen 2R 1K detector. Rietveld refinements were performed using the TOPAS software. SEM images were collected using a Quanta 200 FEG Environmental-SEM in high-vacuum mode. TEM, SAED, EDX, HAADF-STEM, and HR-TEM images were collected on a Talos F200X Scanning/Transmission Electron Microscope with a SuperX EDX detector. Electron diffraction images were simulated using the software CrystalMaker, which also showed the theoretical distances between each diffraction spot. The distances between diffraction spots were measured using the software ImageJ. For atomic force microscopy, samples were drop-cast on silicon wafers and allowed to dry in air. The measurements were performed using a Bruker Dimension Icon3 Atomic Force Microscope in tapping mode and the data was processed using the Gwyddion software. Magnetic measurements were collected in a straw holder on a Quantum Design MPMS 3 using SQUID-VSM.

Author contributions

M. Y. developed the methodology, collected and analyzed the data, and wrote the original and final draft. G. C. and R. S. helped collect and interpret data. N. M. helped validate and interpret the results. F. Y. and L. M. S. conceptualized the idea. N. Y. and L. M. S. supervised the project. All authors reviewed and edited the draft.

Conflicts of interest

There are no conflicts to declare.

Acknowledgements

References

1 J. Bae, M. Kim, H. Kang, T. Kim, H. Choi, B. Kim, H. W. Do and W. Shim, Adv. Mater., 2021, 33, 2006043.

2 A. V. Kolobov and J. Tominaga, Two-Dimensional Transition-Metal Dichalcogenides, Springer, Cham, 2016.

3 B. Mekuye and B. Abera, Nano Select, 2023, 4, 486–501.

4 T. Yasui, T. Yanagida, S. Ito, Y. Konakade, D. Takeshita, T. Naganawa, K. Nagashima, T. Shimada, N. Kaji, Y. Nakamura, I. A. Thiodorus, Y. He, S. Rahong, M. Kanai, H. Yukawa, T. Ochiya, T. Kawai and Y. Baba, Sci. Adv., 2017, 3, e1701133.

5 T. Wasiak and D. Janas, J. Alloys Compd., 2022, 892, 162158.

6 E. Horváth, J. Gabathuler, G. Bourdiec, E. Vidal-Revel, M. Benthem Muñiz, M. Gaal, D. Grandjean, F. Breider, L. Rossi, A. Sienkiewicz and L. Forró, npj Clean Water, 2022, 5, 1–11.

7 M. R. Zamani Kouhpanji and B. Stadler, Part. Part. Syst. Charact., 2021, 38, 2000227.

8 M. R. Zamani Kouhpanji and B. J. H. Stadler, AIP Adv., 2020, 10, 125231.

9 A. Mourachkine, O. V. Yazyev, C. Ducati and J.-P. Ansermet, Nano Lett., 2008, 8, 3683–3687.

10 S. Aryal, D. Paudyal and R. Pati, Nano Lett., 2021, 21, 1856–1862.

11 G. Hrkac, J. Dean and D. A. Allwood, *Philos. Trans. R. Soc., A*, 2011, **369**, 3214–3228.

12 A. May, M. Hunt, A. Van Den Berg, A. Hejazi and S. Ladak, *Commun. Phys.*, 2019, **2**, 1–9.

13 C. Donnelly, A. Hierro-Rodríguez, C. Abert, K. Witte, L. Skoric, D. Sanz-Hernández, S. Finizio, F. Meng, S. McVitie, J. Raabe, D. Suess, R. Cowburn and A. Fernández-Pacheco, *Nat. Nanotechnol.*, 2022, **17**, 136–142.

14 P. C. McIntyre and A. Fontcuberta i Morral, *Mater. Today Nano*, 2020, **9**, 100058.

15 N. P. Dasgupta, J. Sun, C. Liu, S. Brittman, S. C. Andrews, J. Lim, H. Gao, R. Yan and P. Yang, *Adv. Mater.*, 2014, **26**, 2137–2184.

16 J. E. Allen, E. R. Hemesath, D. E. Perea, J. L. Lensch-Falk, Z. Y. Li, F. Yin, M. H. Gass, P. Wang, A. L. Bleloch, R. E. Palmer and L. J. Lauhon, *Nat. Nanotechnol.*, 2008, **3**, 168–173.

17 F. Torrisi and J. N. Coleman, *Nat. Nanotechnol.*, 2014, **9**, 738–739.

18 A. G. Kelly, T. Hallam, C. Backes, A. Harvey, A. S. Esmaeily, I. Godwin, J. Coelho, V. Nicolosi, J. Lauth, A. Kulkarni, S. Kinge, L. D. A. Siebbeles, G. S. Duesberg and J. N. Coleman, *Science*, 2017, **356**, 69–73.

19 X. Song, R. Singha, G. Cheng, Y.-W. Yeh, F. Kamm, J. F. Khoury, B. L. Hoff, J. W. Stiles, F. Pielnhofer, P. E. Batson, N. Yao and L. M. Schoop, *Sci. Adv.*, 2023, **9**, eadd6167.

20 Y. Qu, M. Q. Arguilla, Q. Zhang, X. He and M. Dincă, *J. Am. Chem. Soc.*, 2021, **143**, 19551–19558.

21 P. Topolovsek, C. Gadermaier, D. Vengust, M. Strojnik, J. Strle and D. Mihailovic, *Nano Lett.*, 2015, **15**, 813–818.

22 N. Tian, D. Liu, B. Zhou, Y. Yang, G. Zhang, D. Zhang and Y. Zhang, *Mater. Lett.*, 2018, **228**, 89–91.

23 X. Liu, S. Liu, L. Y. Antipina, Y. Zhu, J. Ning, J. Liu, C. Yue, A. Joshy, Y. Zhu, J. Sun, A. M. Sanchez, P. B. Sorokin, Z. Mao, Q. Xiong and J. Wei, *Nano Res.*, 2020, **13**, 1627–1635.

24 W. Chen, R. Zhang, Y. Sun, J. Wang, Y. Fan and B. Liu, *Adv. Powder Mater.*, 2023, **2**, 100080.

25 B. L. Hoff, G. Cheng, G. Villalpando, F. Yuan, N. Yao and L. M. Schoop, *J. Phys. Mater.*, 2022, **5**, 044004.

26 X. Song, G. Cheng, D. Weber, F. Pielnhofer, S. Lei, S. Klemenz, Y.-W. Yeh, K. A. Filsinger, C. B. Arnold, N. Yao and L. M. Schoop, *J. Am. Chem. Soc.*, 2019, **141**, 15634–15640.

27 T. Chen, H. Kaur, M. McCrystall, R. Tian, A. Roy, R. Smith, D. V. Horvath, J. Maughan, B. Konkena, M. Venkatesan, K. Synnatschke, T. Carey, J. Liu, J. Pepper, R. Zhang, C. Backes, V. Nicolosi, H. Xia and J. N. Coleman, *FlatChem*, 2022, **33**, 100360.

28 C. Gibaja, D. Rodríguez-San-Miguel, W. S. Paz, I. Torres, E. Salagre, P. Segovia, E. G. Michel, M. Assebban, P. Ares, D. Hernández-Maldonado, Q. Ramasse, G. Abellán, J. Gómez-Herrero, M. Varela, J. J. Palacios and F. Zamora, *Adv. Mater.*, 2021, **33**, 2006826.

29 A. Puthirath Balan, S. Radhakrishnan, C. F. Woellner, S. K. Sinha, L. Deng, C. D. L. Reyes, B. M. Rao, M. Paulose, R. Neupane, A. Apte, V. Kochat, R. Vajtai, A. R. Harutyunyan, C.-W. Chu, G. Costin, D. S. Galvao, A. A. Martí, P. A. van Aken, O. K. Varghese, C. S. Tiwary, A. M. M. Ramaswamy Iyer and P. M. Ajayan, *Nat. Nanotechnol.*, 2018, **13**, 602–609.

30 A. P. Balan, A. B. Puthirath, S. Roy, G. Costin, E. F. Oliveira, M. A. S. R. Saadi, V. Sreepal, R. Friedrich, P. Serles, A. Biswas, S. A. Iyengar, N. Chakingal, S. Bhattacharyya, S. K. Saju, S. C. Pardo, L. M. Sassi, T. Filleter, A. Krasheninnikov, D. S. Galvao, R. Vajtai, R. R. Nair and P. M. Ajayan, *Mater. Today*, 2022, **58**, 164–200.

31 F. Cheng, X. Jiang, Z. Zhang, R. Ma, T. Sasaki, F. Pan and X. Jing, *Chem. Commun.*, 2019, **55**, 2417–2420.

32 L. Venkataraman, Y. S. Hong and P. Kim, *Phys. Rev. Lett.*, 2006, **96**, 076601.

33 L. Li, T. Gao, Y. Ge, Q. Zhang, J. Wang, Z. Ma, W. Guo, S. Yu and Y. Fan, *J. Mater. Chem. A*, 2021, **9**, 27727–27735.

34 D. Liang, Y. Chen, S. Zhu, Y. Gao, T. Sun, K. Ri and X. Xie, *Sustainable Environ. Res.*, 2021, **31**, 25.

35 Z. Tomkowicz, A. Szytula and H. Bak-ptasiewicz, *Phys. Status Solidi A*, 1980, **57**, K25–K30.

36 S. K. Tiwary and S. Vasudevan, *Phys. Rev. B: Condens. Matter Mater. Phys.*, 1997, **56**, 7812–7814.

37 W. Bronger, A. Kyas and P. Müller, *J. Solid State Chem.*, 1987, **70**, 262–270.

38 S. K. Tiwary and S. Vasudevan, *Solid State Commun.*, 1997, **101**, 449–452.

39 D. C. Johnston, S. C. Mraw and A. J. Jacobson, *Solid State Commun.*, 1982, **44**, 255–258.

40 D. Kong, J. C. Randel, H. Peng, J. J. Cha, S. Meister, K. Lai, Y. Chen, Z.-X. Shen, H. C. Manoharan and Y. Cui, *Nano Lett.*, 2010, **10**, 329–333.

41 T. Chowdhury, E. C. Sadler and T. J. Kempa, *Chem. Rev.*, 2020, **120**, 12563–12591.

42 F. Wang, N. Mathur, A. N. Janes, H. Sheng, P. He, X. Zheng, P. Yu, A. J. DeRuiter, J. R. Schmidt, J. He and S. Jin, *Sci. Adv.*, 2021, **7**, eabj4086.

43 Q. Li, X. Qian, C. Cheng, B. Kang, S. Cao, J. Zhang and Z. Feng, *Phys. B: Condens. Matter*, 2021, **608**, 412878.

44 C. Guo, H. Li, W. Zhao, J. Pan, T. Lin, J. Xu, M. Chen and F. Huang, *J. Mater. Chem. C*, 2017, **5**, 5977–5983.

45 A. Anto Jeffery, C. Nethravathi and M. Rajamathi, *J. Phys. Chem. C*, 2014, **118**, 1386–1396.

46 J. Peng, Z.-j Chen, B. Ding and H.-M. Cheng, *Research*, 2023, **6**, 0040.

47 E. Lee and D.-J. Kim, *J. Electrochem. Soc.*, 2019, **167**, 037515.

48 J. C. Bonner and M. E. Fisher, *Phys. Rev.*, 1964, **135**, A640–A658.

49 S. Eggert, I. Affleck and M. Takahashi, *Phys. Rev. Lett.*, 1994, **73**, 332–335.

50 S. J. Sebastian, K. Somesh, M. Nandi, N. Ahmed, P. Bag, M. Baenitz, B. Koo, J. Sichelschmidt, A. A. Tsirlin, Y. Furukawa and R. Nath, *Phys. Rev. B*, 2021, **103**, 064413.

51 N. Paunović, Z. V. Popović and Z. D. Dohčević-Mitrović, *J. Phys.: Condens. Matter*, 2012, **24**, 456001.

52 A. Ghosh, S. Paul and S. Raj, *Solid State Commun.*, 2015, **208**, 1–6.

53 T. D. Keene, I. Zimmermann, A. Neels, O. Sereda, J. Hauser, M. Bonin, M. B. Hursthouse, D. J. Price and S. Decurtins, *Dalton Trans.*, 2010, **39**, 4937.

54 W. V. Sweeney and R. E. Coffman, *Biochim. Biophys. Acta, Gen. Subj.*, 1972, **286**, 26–35.

55 R. S. De Biasi and C. A. Taft, *J. Mater. Sci.*, 1978, **13**, 2274–2275.

56 T. Oguchi, *Phys. Rev.*, 1964, **133**, A1098–A1099.

57 D. Alshalawi, J. M. Alonso, A. R. Landa-Cánovas and P. de la Presa, *Nanomaterials*, 2023, **13**, 1657.

58 H. Khurshid, P. Lampen-Kelley, Ò. Iglesias, J. Alonso, M.-H. Phan, C.-J. Sun, M.-L. Saboungi and H. Srikanth, *Sci. Rep.*, 2015, **5**, 15054.

59 K. Momma and F. Izumi, *J. Appl. Crystallogr.*, 2011, **44**, 1272–1276.